Hindawi Publishing Corporation
International Journal of Photoenergy
Volume 2015, Article ID 856385, 10 pages
http://dx.doi.org/10.1155/2015/856385

Research Article

Effects of Dopant Metal Variation and Material Synthesis Method on the Material Properties of Mixed Metal Ferrites in Yttria Stabilized Zirconia for Solar Thermochemical Fuel Production

Jeffrey Leonard,[1] Nichole Reyes,[1] Kyle M. Allen,[1] Kelvin Randhir,[1] Like Li,[1] Nick AuYeung,[2] Jeremy Grunewald,[1] Nathan Rhodes,[1] Michael Bobek,[1] and James F. Klausner[1]

[1]*Department of Mechanical and Aerospace Engineering, University of Florida, Gainesville, FL 32611, USA*
[2]*School of Chemical, Biological and Environmental Engineering, Oregon State University, Corvallis, OR 97331, USA*

Correspondence should be addressed to Like Li; likelichina@ufl.edu and Nick AuYeung; nick.auyeung@oregonstate.edu

Received 1 March 2015; Accepted 31 March 2015

Academic Editor: Fuqiang Wang

Mixed metal ferrites have shown much promise in two-step solar-thermochemical fuel production. Previous work has typically focused on evaluating a particular metal ferrite produced by a particular synthesis process, which makes comparisons between studies performed by independent researchers difficult. A comparative study was undertaken to explore the effects different synthesis methods have on the performance of a particular material during redox cycling using thermogravimetry. This study revealed that materials made via wet chemistry methods and extended periods of high temperature calcination yield better redox performance. Differences in redox performance between materials made via wet chemistry methods were minimal and these demonstrated much better performance than those synthesized via the solid state method. Subsequently, various metal ferrite samples ($NiFe_2O_4$, $MgFe_2O_4$, $CoFe_2O_4$, and $MnFe_2O_4$) in yttria stabilized zirconia (8YSZ) were synthesized via coprecipitation and tested to determine the most promising metal ferrite combination. It was determined that 10 wt.% $CoFe_2O_4$ in 8YSZ produced the highest and most consistent yields of O_2 and CO. By testing the effects of synthesis methods and dopants in a consistent fashion, those aspects of ferrite preparation which are most significant can be revealed. More importantly, these insights can guide future efforts in developing the next generation of thermochemical fuel production materials.

1. Introduction

Solar-thermochemical water (H_2O) and carbon dioxide (CO_2) splitting refers to the stripping away of oxygen (O_2) from H_2O and CO_2 molecules through the use of concentrated solar energy. From this process, molecular hydrogen (H_2) and carbon monoxide (CO) can be extracted. These two products form the building blocks for the production of synthetic hydrocarbon fuels, which are most propitiously produced through the use of the Fischer-Tropsch process [1]. Generating these hydrocarbon based fuels allows for their straightforward dispersal through the use of established transportation fuel distribution networks, all while maintaining carbon neutrality. Moreover, forming liquid fuels in this fashion allows for the storage of concentrated solar thermal energy in a form that allows for easy transport and storage. This method provides a means of efficiently transporting clean solar energy from regions of intense solar insolation to areas with poor solar resources, a problem faced by the direct production of electricity via solar energy. These benefits make thermochemical H_2O and CO_2 splitting a promising field of research [2, 3].

The direct solar thermolysis of H_2O and CO_2 occurs in significant quantities at temperatures greater than 2500 K [4, 5]. These extreme temperatures present an overwhelming obstacle in the selection of reactor materials and reactor design. To overcome this hurdle, a two-step oxidation-reduction cycle utilizing metal oxides is often employed [6, 7].

This cycle operates at much more favorable temperatures and functions by converting a metal or low-valence state metal oxide to a greater oxidation state by sequestering O_2 from H_2O or CO_2 molecules. The H_2 or CO liberated from the oxidation step can then be collected. In the second step, the metal oxide is thermally reduced back to its original state through the use of concentrated solar energy. The corresponding reactions are as follows.

Oxidation by H_2O:

$$M_xO_{y-1} + H_2O \longrightarrow M_xO_y + H_2 \quad (1)$$

Oxidation by CO_2:

$$M_xO_{y-1} + CO_2 \longrightarrow M_xO_y + CO \quad (2)$$

Thermal reduction:

$$M_xO_y \longrightarrow M_xO_{y-1} + \frac{1}{2}O_2 \quad (3)$$

A great deal of interest has been generated towards determining which metal oxide material has the greatest potential for efficient H_2 and/or CO production. Several different metal oxides have been studied in previous works. While iron oxides have been perhaps the most well studied of them all [8–11], these materials have exhibited problems with maintaining active surface area, as iron oxides tend to sinter extensively at the high temperatures when performing repeated redox cycling [12–14]. This adversely affects the reactivity of the redox material. Previous work has shown that ferrite particles supported by zirconium oxide (ZrO_2) exhibit a lesser degree of sintering and thus greater cycling longevity [15, 16]. Yet, the inclusion of ZrO_2 presents a new issue. Pure ZrO_2 undergoes phase transformations from monoclinic (stable phase at room temperature) to tetragonal (at around 1000°C) and finally to cubic (at approximately 2370°C). These crystallographic orientation changes are accompanied by significant volume variations that result in microstructural fracturing during redox cycling. To combat this, ZrO_2 can be stabilized in the cubic phase through the addition of yttrium oxide (Y_2O_3). The resulting yttria stabilized zirconia (YSZ) is no longer prone to fracture from crystallographic transformations in the temperature range of interest.

Previous works have found considerable success doping iron oxide with a second metallic cation, such as Zn, Ni, Mn, or Co [15, 17–22]. Ferrites doped with Ni, Mn, or Co have exhibited an increase in reaction rates and have required lower temperatures for reduction [16, 23–25]. Moreover, these doped ferrites tend to have higher melting points, thus lowering the rate of sintering during the reduction step [26]. Mn doped ferrite shows significant potential for H_2O splitting, as its performance has shown to be quite favorable in both the reduction and oxidation steps [27]. In the present work, ferrite materials with 10 wt.% of different dopant metals, including Ni, Mn, Mg, and Co, in 8 mol.% yttria stabilized zirconia ($(Y_2O_3)_{0.08}(ZrO_2)_{0.92}$, henceforth referred to as 8YSZ) are examined as reactive materials for repeated two-step cyclic CO_2 splitting.

It is noted that much of the previous literature on this subject focuses on the characterization of a particular material and its performance during redox cycling. Furthermore, these studies often utilize only one specific material synthesis process. The variability between studies often makes comparisons difficult. The primary purpose of this paper is to (1) explore the effects of different synthesis methods of one specific material (manganese ferrite in 8YSZ) on the performance of the material during redox cycling (thermal reduction and CO_2 splitting) and (2) present a comparative analysis of the performance of different mixed metal ferrites in 8YSZ. The second part of this study will seek to determine the most suitable metal ferrite for thermochemical CO_2 splitting.

2. Experimental Methods

2.1. Synthesis Methods. In efforts to develop the material with the greatest productivity, several synthesis methods have been used. One such method is liquid phase self-propagating high temperature synthesis (LPSHS). This method of synthesizing inorganic compounds was first studied in the early 1970s [28]. Material synthesis occurs via self-sustaining combustion reactions in precursor solutions of metal nitrates and soluble organic fuels. Synthesis of solid-phase materials in the liquid phase allows for the interspersing of reactants on a molecular level and has been demonstrated to yield more homogenous results [29]. One drawback of this method is the presence of organic compounds in the synthesized powders. This requires a postprocessing step to remove these substances from the material [30].

Another synthesis method used extensively in literature is the sol-gel method. This method of synthesizing metal oxides operates by forming a gel of cross-linked polymers of metals and organic oxides from a solution. It is a low temperature process and is known to yield products with a high specific surface area. Moreover, the gelation process takes place in solution, allowing for better molecular interaction and thus more homogenous results. These attributes make the sol-gel method extremely promising [31].

The third method to be explored is the coprecipitation method. This method is the simplest to implement of the three wet chemistry synthesis methods. Metal nitrates, chlorides, or sulfates are dissolved in deionized water. A strong base is then used to initiate precipitation of the metal hydroxides. Again, the aqueous nature of this process allows for significant molecular mixing and thus a more homogenous material [5].

Finally, a fourth control sample is generated using solid state synthesis. Previous literature suggests that solid state synthesis has lower O_2 mobility characteristics than other synthesis methods [29].

Upon the synthesis of the manganese ferrite samples, the samples will be heat treated in a process referred to as calcination. The purpose of the calcination step is to prepare the amorphous, homogenized samples for high temperature redox reactions. Calcination promotes increased crystallinity of the materials, bringing the material into a form more closely resembling that which would be formed during extended redox cycling.

The four material synthesis procedures outlined above were exercised to produce 10 wt.% metal ferrites in 8YSZ. The details for making the 10 wt.% $MnFe_2O_4$ in 8YSZ are presented below.

To eliminate the introduction of material impurity based inconsistencies between samples, the same metal nitrate stock compounds were used in each method. Yttrium (III) nitrate hexahydrate ($Y(NO_3)_3{\cdot}6H_2O$, Fischer Scientific), iron (III) nitrate nonahydrate ($Fe(NO_3)_3{\cdot}9H_2O$, Fischer Scientific), manganese (II) nitrate tetrahydrate ($Mn(NO_3)_2{\cdot}4H_2O$, Fischer Scientific), and a solution of 35 wt.% zirconyl nitrate in dilute nitric acid (Sigma-Aldrich) were utilized to provide the metal cations for each reaction.

2.1.1. Synthesis of $MnFe_2O_4$ in 8YSZ via Coprecipitation. Stoichiometric quantities of the various metal nitrate compounds were measured so as to obtain 10 g of 10 wt.% $MnFe_2O_4$ in 8YSZ. The nitrates were added to 1000 mL of deionized water and placed on a hot plate (Corning) set to 60°C. A pH meter (9124N, Hanna Instruments) and thermocouple (Corning) were placed in the solution. In a separate beaker, a solution of 80 mL ammonium hydroxide and 500 mL deionized water were heated to approximately 60°C on a separate hot plate. Magnetic stirring rods were added to each beaker and set to 260 rpm. Upon reaching 60°C the ammonium hydroxide solution was added to the metal nitrate solution in a dropwise fashion allowing the system to slowly reach equilibrium. This was repeated until the nitrate solution reached a pH of 8.5. The resulting precipitate was then separated from the supernate through vacuum filtration. The resulting filtered material was then placed in a drying oven at 150°C for 24 hours.

2.1.2. Synthesis of $MnFe_2O_4$ in 8YSZ via Sol-Gel Method. Stoichiometric quantities of the various metal nitrate compounds were measured so as to obtain 10 g of 10 wt.% $MnFe_2O_4$ in 8YSZ. The resulting nitrates were added to 20 mL of ethanol in a closed-top and air-tight Teflon jar and ultrasonicated until a complete dissolution of the metal nitrates was achieved. 16 mL of propylene oxide (CH_3CHCH_2O, 99%+ Sigma-Aldrich) was then slowly added to the solution in a dropwise fashion over a period of 1-2 minutes. This addition was performed under a chemical hood to prevent inhalation of the propylene oxide fumes. At the conclusion of this step, the lid for the jar was secured and the formation of gel was observed. The gel was allowed to rest for 24 hours and then placed in an oven at 105°C for 24 hours for gel aging.

2.1.3. Synthesis of $MnFe_2O_4$ in 8YSZ via LPSHS. Stoichiometric quantities of the various metal nitrate compounds were measured so as to obtain 10 g of 10 wt.% $MnFe_2O_4$ in 8YSZ. The samples were then dissolved in 50–100 mL of deionized water in a 2 L beaker. Citric acid (2.8 M) was added to the mixture in a 3 to 1 molar ratio of metal cations to citric acid. Citric acid was chosen as the fuel due to its ability to form chelate complexes with all metal ions, thus allowing for a homogenous precipitation. Dilute ammonium hydroxide was added to the solution until a pH of 7 was reached. The addition of the ammonium nitrate supplies the amine needed to form ammonium nitrate with the nitrates from the dissolved metal nitrates. It also ensures a high level of chelation of all cations. The solution was then heated to 80°C and stirred constantly until a gel formed. At this point, heating was steadily increased to 550°C until the material self-ignited and fully combusted. The resulting ash was collected.

2.1.4. Solid State Synthesis. 8YSZ in the form of a plasma spray powder, MnO, and Fe_2O_3 powders were mixed together to achieve 10 g of 10 wt.% $MnFe_2O_4$ in 8YSZ. To ensure a high level of interspersing of materials, the powders were ground and mixed via mortar and pestle.

2.2. Preparation of Metal Ferrites with Different Dopants. Samples of 10 wt.% $MnFe_2O_4$ in 8YSZ, 10 wt.% $NiFe_2O_4$ in 8YSZ, 10 wt.% $MgFe_2O_4$ in 8YSZ, and 10 wt.% $CoFe_2O_4$ in 8YSZ were synthesized utilizing the coprecipitation method.

2.3. Calcination and Pellet Formation. The powders from the four synthesis methods were crushed separately via a zirconia mortar and pestle. To create porous structures for each sample, 1.3 g of metal oxide powders was mixed with 0.4 g of 300 mesh graphite powder and 0.8 g of 100 mesh graphite powder. A binder solution of 3.5 wt.% polyethylene glycol (PEG) and 3.5 wt.% polyvinyl alcohol (PVA) in deionized water was prepared and added to the samples to help retain their structure. For each 2.5 g sample, binder solution was added to the powder until incipient wetness occurred. This slurry was dried in air and the resulting powder was then pressed into a 20 mm diameter pellet to a pressure of 10 tons. To burn out the binding agent, the pellet was taken to 600°C at $1°C\,min^{-1}$ and then returned to ambient conditions without dwelling at a rate of $1°C\,min^{-1}$. After binder burnout, each pellet was calcined at 1350°C for 36 hours and then ramped up to 1450°C for 4 hours. Temperature ramps during this step were $5°C\,min^{-1}$. This step allowed the carbon pore former to oxidize, leaving voids left behind by carbon.

A portion of each sample was tested in the CO_2 splitting redox cycle via thermogravimetric analysis (TGA) using a Netzsch 449 F3 simultaneous thermal analyzer (STA; NETZSCH Instruments North America, LLC, Burlington, MA). The oxidation and reduction steps executed in the TGA were performed at 1100°C and 1450°C, respectively, for a total of 5 cycles of oxidation and reduction. Reduction was performed at a temperature of 1450°C for a period of 120 minutes under inert argon gas flowing at $140\,cm^3\,min^{-1}$. Oxidation was performed by flowing $120\,cm^3\,min^{-1}$ of CO_2 and $20\,cm^3\,min^{-1}$ of argon for 90 minutes at a temperature of 1100°C. The ramp up and ramp down rates for both steps are $50°C\,min^{-1}$.

3. Results and Discussion

3.1. Synthesis Method Investigation

3.1.1. XRD Analysis. To develop an understanding of each material structure and to confirm proper synthesis, powder

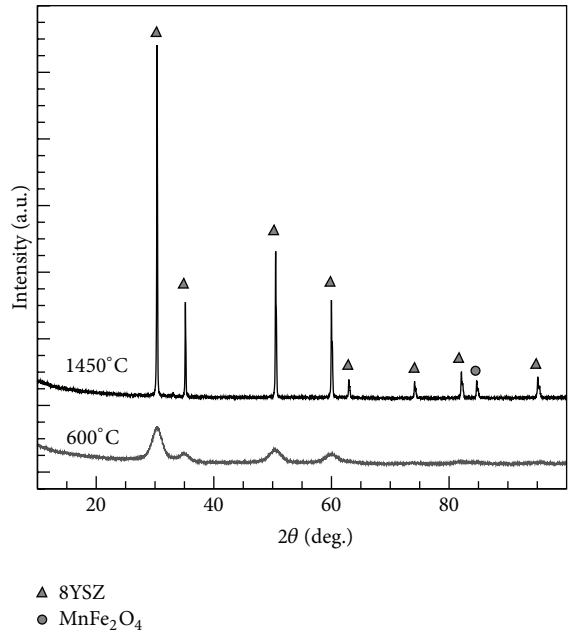

Figure 1: Precalcination (600°C) and postcalcination (1450°C) XRD for sol-gel derived $MnFe_2O_4$ in 8YSZ.

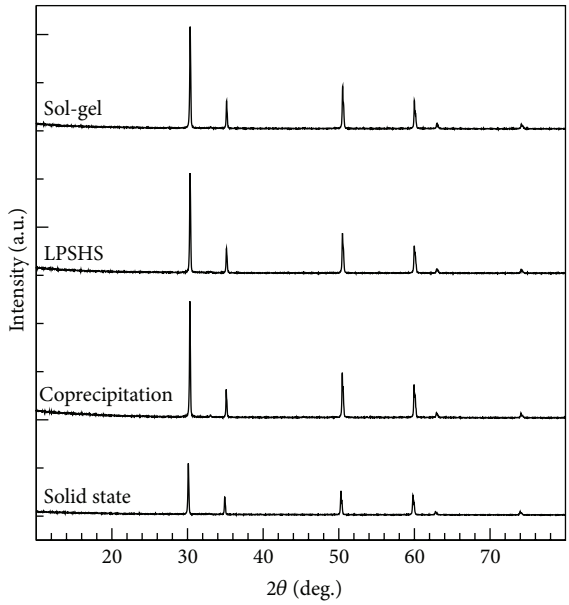

Figure 2: Postcalcination XRD for $MnFe_2O_4$ samples created using four different synthesis methods.

X-ray diffraction (XRD) analysis was performed on each material prior to calcination and postcalcination. Figure 1 shows the pre- and postcalcination XRD analysis of the material prepared with sol-gel method.

From Figure 1 it can be seen that the postsynthesis material has much narrower and intense peaks than the precalcination sample. This shows that the material is much more amorphous than its postcalcination sample. It also indicates that the calcination procedure is critical to achieving a crystalline structure. The postcalcination XRD data for the four different samples are presented in Figure 2.

The postcalcination XRD patterns of the top three samples shown in Figure 2 were prepared via a wet route and show that all three substances are the same material with similar grain size, density, and structure. The sol-gel and LP SHS methods appear to have extremely similar intensities and band thicknesses indicating similar crystal size. The coprecipitation method has the highest and most narrow peaks suggesting this method yielded the smallest crystallites. The solid state method has the lowest XRD peak intensities, indicating it is the least crystalline material.

The crystal structure change of the samples during the reduction-oxidation cycles is not visible since the temperatures for both steps did not go above the calcination temperature. In addition, the mass ratio of the reactive ferrite is only 10 wt.% and the majority is 8YSZ. Thus the XRD pattern is almost identical for the samples before and after multiple reduction-oxidation cycles.

3.1.2. SEM and EDS Mapping. To further characterize the materials generated, scanning electron microscope (SEM) and energy dispersive spectrometry (EDS) images were developed for each sample after synthesis and then again after calcination. Figure 3 compares the SEM and EDS images of the sol-gel sample prior to calcination and then after calcination. Figure 4 displays the SEM and EDS images of the sample prepared via the solid state method after calcination. The solid state sample was in powder form before calcination and thus no SEM was conducted at that stage. As seen in the EDS images of Figure 3, the sol-gel sample was extremely homogenous directly after synthesis. After calcination, this same sample showed a segregated material with clearly different phases. This same trend was seen in the other two samples synthesized via wet chemistry methods. These results indicate that the high temperature calcination procedure fosters segregation of the iron and manganese in clusters separate from the yttria stabilized zirconia.

The solid state sample exhibited similar segregation in the postcalcination sample (Figure 4), but the clusters of manganese and iron were larger (see Figures 3 and 4 magnifications) and appear to be less evenly distributed than those prepared using wet chemistry methods. This is most likely due to the solid state synthesis method producing a less homogenous sample prior to calcination relative to the wet methods. The poor distribution of materials allowed for larger clusters to form in the solid state sample.

It can be postulated that if these materials were not calcined and directly tested in two-step thermochemical CO_2 splitting, the first few oxidation and reduction steps would occur in a transient stage as the material structure moves towards its pseudosteady state shown in the postcalcination EDS images. From characterization, it can be seen that the calcination procedure has a significant effect on the material structure. Due to this profound effect, further study is needed to determine optimal temperatures and dwell times for calcination.

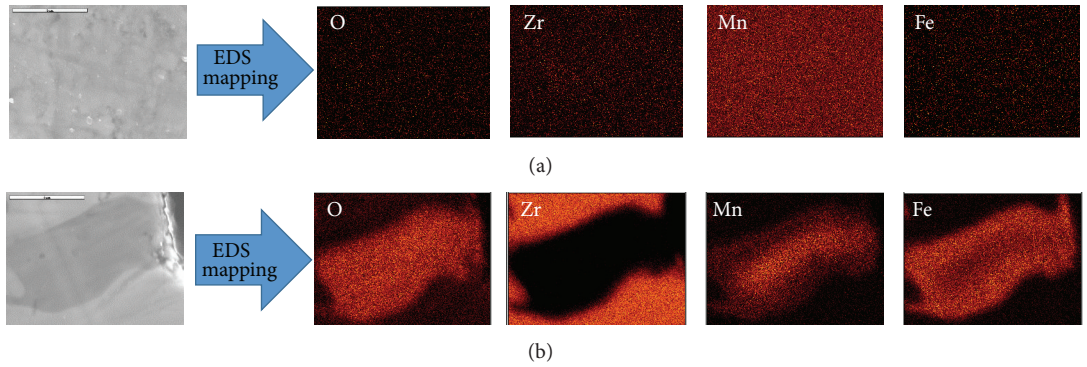

FIGURE 3: Sol-gel sample before (a) and after (b) calcination. SEM and EDS mapping at 10,000x magnification (the length of the scale bars in the SEM images is 5 μm).

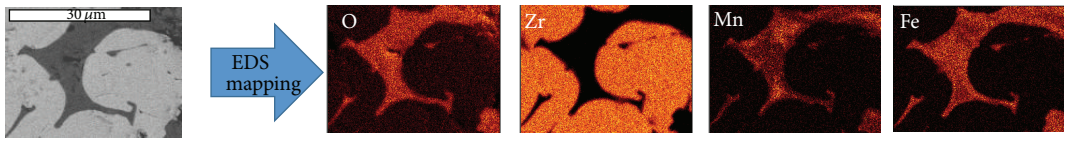

FIGURE 4: Solid state sample after calcination. SEM and EDS mapping at 3,000x magnification (the length of the scale bar in the SEM image is 30 μm).

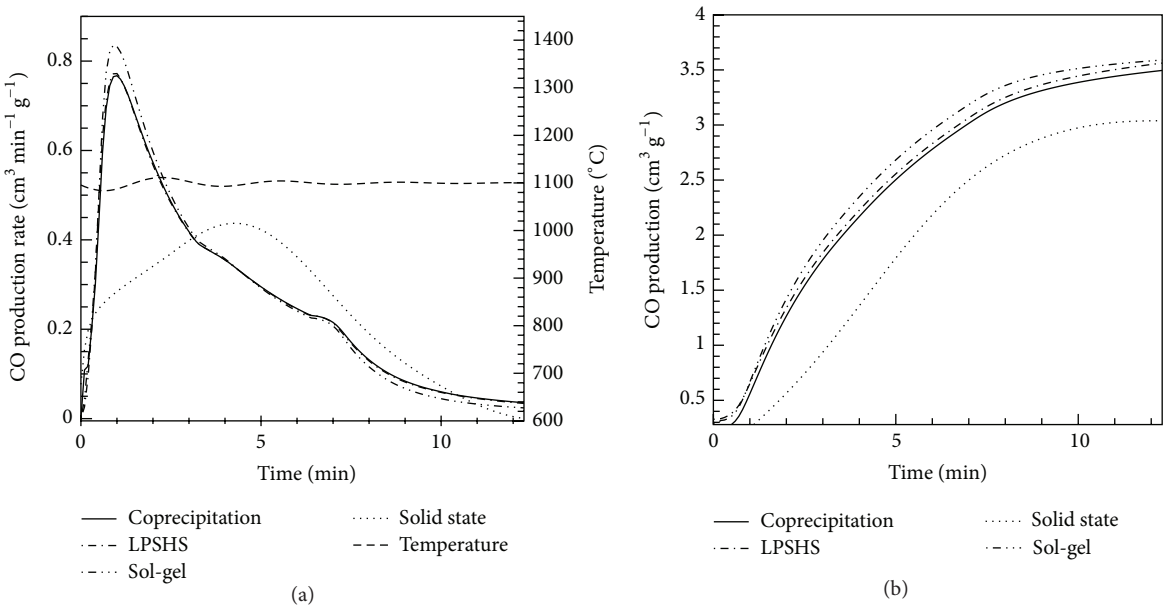

FIGURE 5: CO production (a) rate and (b) yield versus time during the oxidation step of the 5th cycle.

3.1.3. Thermogravimetric Analysis. The thermogravimetric results from the three samples of 10 wt.% $MnFe_2O_4$ in 8YSZ made via wet chemistry methods had similar rates and overall yields. The overall mass changes for the five cycles are presented in Figure S1 of the Supplementary Material available online at http://dx.doi.org/10.1155/2015/856385. The CO production rate ($cm^3\ min^{-1}\ g^{-1}$ of total material) and its cumulative yield ($cm^3\ g^{-1}$ of total material) versus oxidation time for all samples during the 5th cycle are presented in Figures 5(a) and 5(b), respectively. The production rate for each case dropped to a very small value close to zero after 12.5 min and the corresponding yield reached the steady state. As shown in Figure 5(a), the performance of solid state pellet during oxidation was significantly more gradual than the other materials. Moreover, from Figure 5(b) it can be seen that the solid state pellet had a lower overall yield than the other materials. The sol-gel sample had the highest peak rate and largest overall yield; however, all three materials prepared with wet

Table 1: CO and O_2 yield for the 5th cycle for the four samples prepared with different synthesis methods.

Synthesis method	O_2 yield [$cm^3\ g^{-1}$]	CO yield [$cm^3\ g^{-1}$]	Ratio ($CO : O_2$)
Solid state	1.579	3.038	1.897
Coprecipitation	1.878	3.547	1.889
Sol-gel	1.763	3.711	2.105
LPSHS	1.847	3.687	1.995

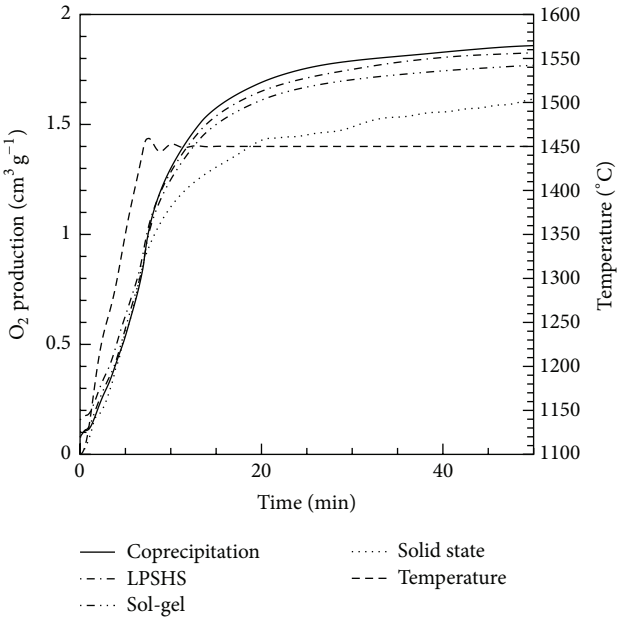

Figure 6: O_2 production versus time during the reduction step of the 5th cycle.

chemistry exhibited very similar results for both the rates and yield of CO production (see also the results in Table 1). In addition, the yield of O_2 ($cm^3\ g^{-1}$ of total material) for the 5th thermal reduction cycle is shown in Figure 6, where very similar results are observed for the three samples prepared with wet chemistry synthesis methods. The rates and yield are much higher than those recorded for the solid state sample.

After multiple cycles of oxidation and reduction, the performance of all material samples slightly declined. From the first cycle to the fifth cycle the performance of each sample declined by about 2%. This is most likely caused by a small amount of sintering. Overall, the samples seemed to be fairly resistant to sintering and maintained similar performance between cycles.

The CO and O_2 yield for the 5th cycle for all four samples are summarized in Table 1, where the ratio between CO and O_2 yield is also included (the theoretical value for the ratio is 2).

From Table 1 it can again be noted that the sample prepared with the solid state method significantly underperformed when compared to its counterparts synthesized via wet chemistry. The solid state sample on average produced 15% less CO and 12.5% less O_2 than the wet chemistry methods. In addition it can be seen that the three samples formed via a wet chemistry route achieved similar results. The wet chemistry samples produced CO yield within 5% of each other and O_2 yield within 6% of each other (in reference to the respective highest values).

3.1.4. Calcination Study. The results of the material synthesis investigation showed that there was no significant difference in the performance of materials prepared via wet methods. It was then postulated that perhaps the calcination step had greater significance, provided the material was produced via a wet chemistry synthesis method. With this in mind, it must be determined whether the maximum calcination temperature or the dwell time at that temperature is the factor driving the resulting material structure. To further explore this idea, several samples of 10 wt.% $CoFe_2O_4$ in 8YSZ were created via the coprecipitation method and then subjected to different calcination procedures that varied in both time and temperature. One of these samples was calcined at 1200°C for 48 hours (a comparatively lower temperature but a long dwell time), another was calcined at 1500°C for 2.5 hours (a higher temperature but a short dwell time), and finally a third sample was produced via the calcination procedure outlined in Section 2.3 (the normal procedure utilizes both high temperature and a long dwell time). After calcination each sample was tested using the two-step thermochemical CO_2 splitting process for five cycles under the same operational conditions as described earlier. The overall mass changes for the five cycles are presented in Figure S2 of the Supplementary Material. Figures 7(a) and 7(b) show the respective CO production rate and yield for the three samples via different calcination methods during the oxidation step of the 4th cycle.

As noticed from Figure 7(a), the sample that underwent calcination at both a high temperature and with long dwell time ("1350°C 36 hr and 1450°C 4 hr") has a significantly higher CO production peak rate than the samples with low temperature, long dwell time ("1200°C 48 hr"), and high temperature, short dwell time ("1500°C 2.5 hr"). This provides evidence that both calcination temperature and dwell time play a crucial role in the fuel production capability of the material. This conclusion is also supported with the analysis of the cumulative CO and O_2 yield shown in Figures 7(b) and 8, respectively.

The results in Figures 7 and 8 clearly show that the high temperature and long dwell time material produced the highest yield and continued to increase in production after the other samples had stabilized.

The results of this study demonstrate that the calcination procedure has a controlling effect on material performance in two-step CO_2 splitting. Furthermore, it can be seen that calcination at high temperature and for long dwell times produces materials that generate the greatest CO and O_2 production rates and overall yield.

3.1.5. Summary of Synthesis Method Study. Three different wet chemistry synthesis methods and one solid state synthesis method were used to develop 10 wt.% $MnFe_2O_4$ in 8YSZ

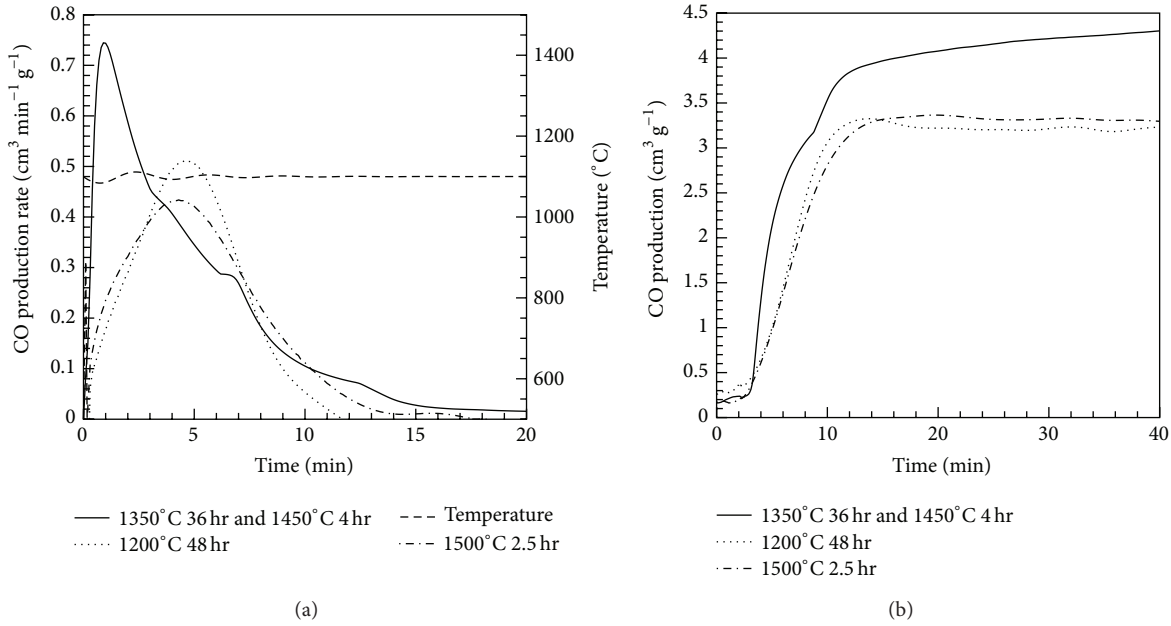

FIGURE 7: CO production (a) rate and (b) yield versus time during the oxidation step of the 4th cycle.

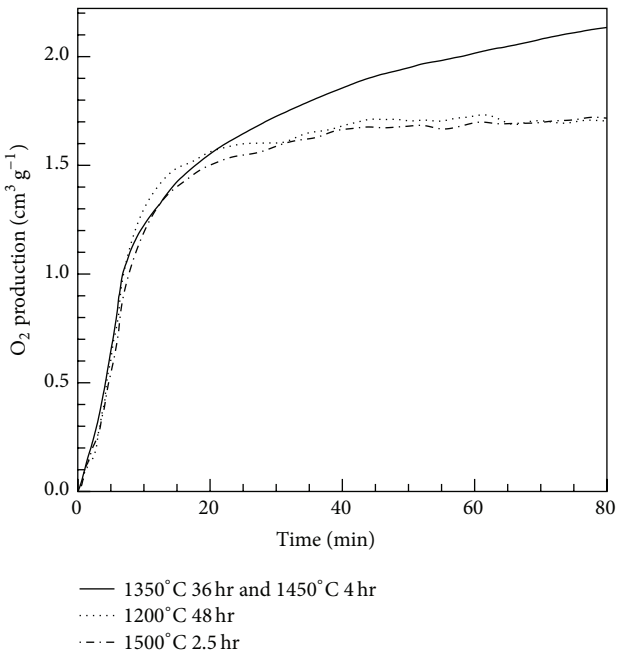

FIGURE 8: O_2 production versus time during the reduction step of the 4th cycle.

for use in a two-step thermochemical CO_2 splitting process for fuel production. From X-ray diffraction patterns and scanning electron microscope images it can be seen that all three wet chemistry methods yielded almost identical materials. Moreover, performance of samples made via these three wet methods in the two-step CO_2 splitting process was markedly similar. Comparable reduction and oxidation rates as well as O_2 and CO yields were observed across these samples. In addition, all three samples outperformed the solid state synthesis sample in both rates and yields in the redox cycling. From these results it can be concluded that, for 10 wt.% $MnFe_2O_4$ in 8YSZ, wet synthesis methods yield better results than samples made via solid state synthesis. In addition, from the EDS mapping of the samples prior to calcination and postcalcination, it can be seen that the calcination procedure is extremely important in material synthesis. Other authors have presented data showing materials exhibiting excellent performance in the first few redox cycles and a decreasing yield in subsequent cycles. It can be concluded that this is most likely due to the material moving towards its postcalcination structure.

With the identification of the most promising calcination procedure and determining that the three wet chemistry methods yield similar results, a study seeking to determine the most promising mixed metal ferrite can now be developed.

3.2. Doped Metal Ferrite Study. Several distinct metal ferrites have been analyzed in the literature [5, 15, 16, 20, 22, 24, 26, 27, 32]; of these, $NiFe_2O_4$, $CoFe_2O_4$, and $MnFe_2O_4$ have been predominant. However, surprisingly no rigorous study has been performed to compare several of these mixed metal ferrites under the same experimental circumstances. Utilizing the findings from the previous section on the comparison of different synthesis methods, a comparative analysis of the redox capabilities of four different doped ferrites, including $CoFe_2O_4$, $MgFe_2O_4$, $NiFe_2O_4$, and $MnFe_2O_4$ in 8YSZ, was performed to determine the most suitable metal ferrite for thermochemical CO_2 splitting. All samples were synthesized utilizing the coprecipitation method and calcined using the high temperature, long dwell time method outlined in Section 2.3. The XRD data for the four samples are shown

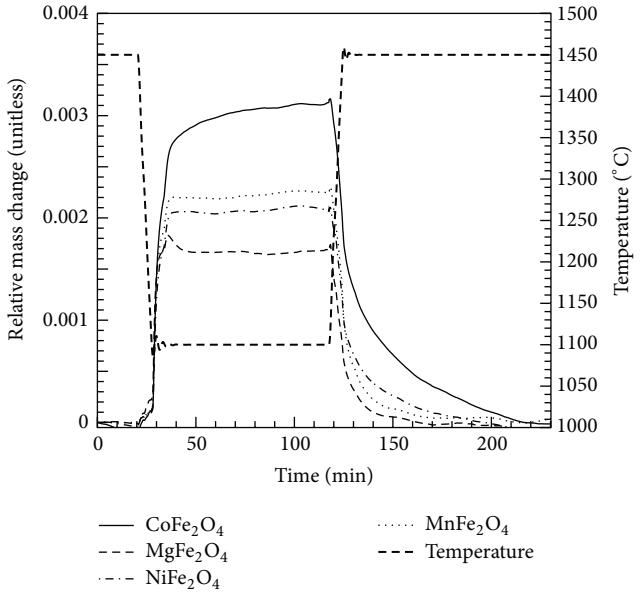

Figure 9: Normalized mass change of all samples for the 5th cycle.

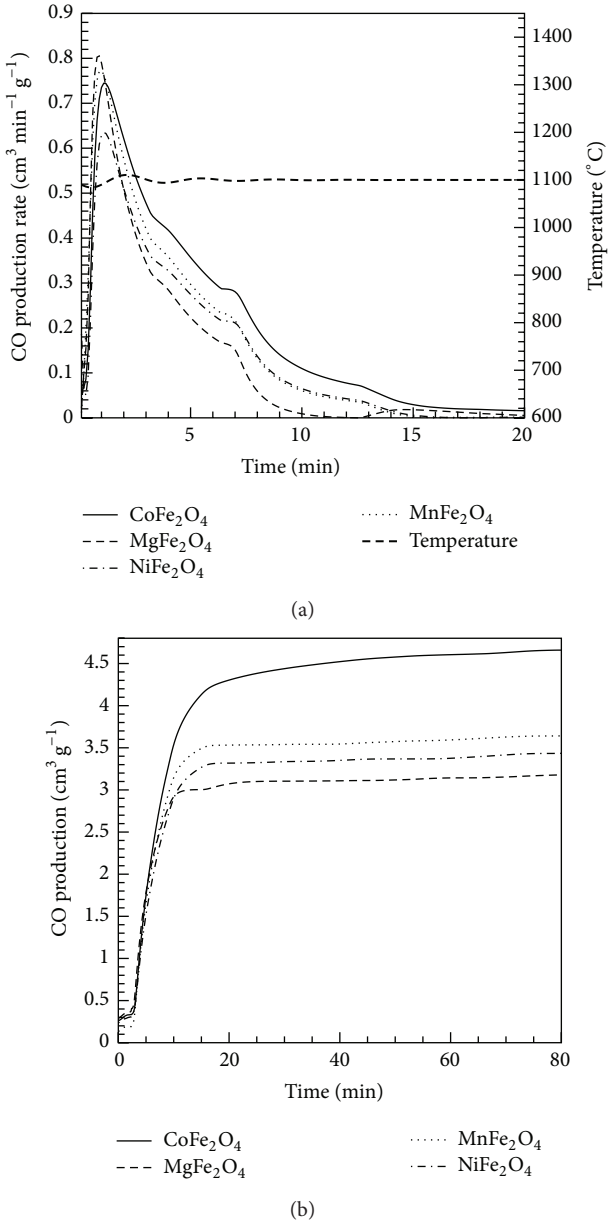

Figure 10: CO production (a) rate and (b) yield of all samples at the 5th cycle.

in Figure S3 of the Supplementary Material. A portion of each sample was tested in the CO_2 splitting redox cycle via thermogravimetric analysis utilizing the same 5-cycle scheme as in the previous section. Figure S4 in the Supplementary Material shows the mass changes for the 5 cycles of the four samples.

The relative mass change compared to the initial mass for each sample during the 5th cycle is presented in Figure 9. From this figure it can be seen that the $CoFe_2O_4$ sample achieved the greatest relative mass change between the oxidation and reduction steps. This indicates that it will have the greatest yields of CO and O_2. Moreover, Figure 9 shows that the $MgFe_2O_4$ sample had the smallest relative mass change between the oxidation and reduction steps and thus will have the lowest overall yields of CO and O_2.

Figure 10(a) displays the CO production rate during the 5th cycle for each of the four samples. The greatest CO production peak rate was observed for $MgFe_2O_4$; however, it quickly dropped off within 2 minutes and showed the lowest production rate. After the initial peak the $CoFe_2O_4$ sample maintained higher CO production rates than any of the other three samples. The cumulative CO production yield for the 5th cycle is presented in Figure 10(b), which clearly shows that the $CoFe_2O_4$ sample achieved the highest overall yield.

The O_2 production yield versus time for the four samples during the reduction step of the 5th cycle is shown in Figure 11, where it is clear that the $CoFe_2O_4$ sample produced the greatest yield by a considerable difference and the $MnFe_2O_4$ sample produced the second largest O_2 yield. The superior reduction extent of $CoFe_2O_4$ is supported in the results of other papers [15, 32].

The total CO and O_2 yield for each sample during the 5th cycle were presented in Table 2. From this table it is evident that the 10 wt.% $CoFe_2O_4$ in 8YSZ sample possesses the highest reduction and oxidation capabilities out of all the samples tested. The $MgFe_2O_4$ sample, on the other hand, provided the lowest O_2 and CO yields.

4. Conclusions

Following the study on different synthesis methods, a comparative analysis on the redox performance of four mixed metal oxides was performed. Cobalt ferrite, magnesium ferrite, nickel ferrite, and manganese ferrite in yttria stabilized zirconia were analyzed using thermogravimetric analysis for a total of five redox cycles. The results indicate that cobalt ferrite produces the highest O_2 and CO yield out of all the other samples under the same conditions. The material also

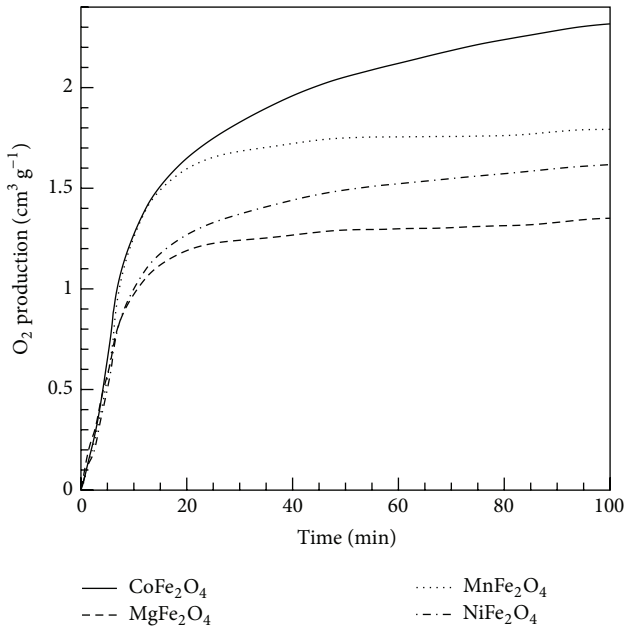

Figure 11: O_2 production of all samples at the 5th cycle.

Table 2: CO and O_2 yield for the 5th cycle for the four different mixed metal ferrites in 8YSZ.

Sample	Initial mass (mg)	O_2 yield [$cm^3\ g^{-1}$]	CO yield [$cm^3\ g^{-1}$]	Ratio ($CO : O_2$)
$CoFe_2O_4$	98.97	2.321	4.706	2.027
$MgFe_2O_4$	102.64	1.358	3.209	2.364
$MnFe_2O_4$	102.14	1.809	3.657	2.022
$NiFe_2O_4$	101.81	1.619	3.484	2.152

demonstrated stable cyclability and a desirable production for both O_2 and CO throughout all 5 cycles.

Since the type of wet chemistry synthesis method chosen for metal ferrite materials was shown to play little role in its performance in the two-step CO_2 splitting process, the deciding factor in determining the most suitable synthesis method for this group of materials should now be based off of economic viability, scalability, and conformance to the 12 principles of green chemistry. Certain methods may be easier to implement on an industrial scale than others. The calcination time and temperature were demonstrated to have a significant influence on the productivity of the material. Reasons for this could include enhanced stability and better homogeneity of the mixed metals in 8YSZ.

A comparative study of multiple materials under the same operational conditions leads to data that is more coherent and easier to draw conclusions from. In order to further examine synthesis methods, the approaches used in this study should be applied to a wider range of materials including next generation thermochemical H_2O and CO_2 splitting materials. Based on the present study, a more comprehensive knowledge of the role that synthesis methods play in material reactivity can be achieved.

Conflict of Interests

The authors declare that there is no conflict of interests regarding the publication of this paper.

Acknowledgment

This paper was prepared with the support of the US Department of Energy, ARPA-E, under Award no. DE-AR0000184.

References

[1] T. Riedel and G. Schaub, "Low-temperature Fischer-Tropsch synthesis on cobalt catalysts—effects of CO_2," *Topics in Catalysis*, vol. 26, no. 1–4, pp. 145–156, 2003.

[2] C. L. Muhich, B. W. Evanko, K. C. Weston et al., "Efficient generation of H2 by splitting water with an isothermal redox cycle," *Science*, vol. 341, no. 6145, pp. 540–542, 2013.

[3] W. C. Chueh, C. Falter, M. Abbott et al., "High-flux solar-driven thermochemical dissociation of C_{O2} and H_2O using nonstoichiometric ceria," *Science*, vol. 330, no. 6012, pp. 1797–1801, 2010.

[4] E. A. Fletcher and R. L. Moen, "Hydrogen and oxygen from water," *Science*, vol. 197, no. 4308, pp. 1050–1056, 1977.

[5] A. J. Traynor and R. J. Jensen, "Direct solar reduction of CO_2 to fuel: first prototype results," *Industrial and Engineering Chemistry Research*, vol. 41, no. 8, pp. 1935–1939, 2002.

[6] K. M. Allen, E. N. Coker, N. Auyeung, and J. F. Klausner, "Cobalt ferrite in YSZ for use as reactive material in solar thermochemical water and carbon dioxide splitting. Part I. Material characterization," *JOM*, vol. 65, no. 12, pp. 1670–1681, 2013.

[7] A. Steinfeld, "Solar thermochemical production of hydrogen—a review," *Solar Energy*, vol. 78, no. 5, pp. 603–615, 2005.

[8] R. B. Diver, J. E. Miller, M. D. Allendorf, N. P. Siegel, and R. E. Hogan, "Solar thermochemical water-splitting ferrite-cycle heat engines," *Journal of Solar Energy Engineering*, vol. 130, no. 4, Article ID 041001, 8 pages, 2008.

[9] C. Agrafiotis, M. Roeb, and C. Sattler, "A review on solar thermal syngas production via redox pair-based water/carbon dioxide splitting thermochemical cycles," *Renewable and Sustainable Energy Reviews*, vol. 42, pp. 254–285, 2015.

[10] J. E. Miller, A. H. McDaniel, and M. D. Allendorf, "Considerations in the design of materials for solar-driven fuel production using metal-oxide thermochemical cycles," *Advanced Energy Materials*, vol. 4, no. 2, Article ID 1300469, 2014.

[11] S. Abanades and I. Villafan-Vidales, "CO_2 valorisation based on Fe_3O_4/FeO thermochemical redox reactions using concentrated solar energy," *International Journal of Energy Research*, vol. 37, no. 6, pp. 598–608, 2013.

[12] S. Fukase and T. Suzuka, "Residual oil cracking with generation of hydrogen: deactivation of iron oxide catalyst in the steam-iron reaction," *Applied Catalysis A, General*, vol. 100, no. 1, pp. 1–17, 1993.

[13] P. C. Knight, J. P. K. Seville, H. Kamiya, and M. Horio, "Modelling of sintering of iron particles in high-temperature gas fluidisation," *Chemical Engineering Science*, vol. 55, no. 20, pp. 4783–4787, 2000.

[14] E. N. Coker, A. Ambrosini, M. A. Rodriguez, and J. E. Miller, "Ferrite-YSZ composites for solar thermochemical production

of synthetic fuels: in operando characterization of CO_2 reduction," *Journal of Materials Chemistry*, vol. 21, no. 29, pp. 10767–10776, 2011.

[15] T. Kodama, Y. Kondoh, R. Yamamoto, H. Andou, and N. Satou, "Thermochemical hydrogen production by a redox system of ZrO_2-supported Co(II)-ferrite," *Solar Energy*, vol. 78, no. 5, pp. 623–631, 2005.

[16] T. Kodama, N. Gokon, and R. Yamamoto, "Thermochemical two-step water splitting by ZrO_2-supported $Ni_xFe_{3-x}O_4$ for solar hydrogen production," *Solar Energy*, vol. 82, no. 1, pp. 73–79, 2008.

[17] T. Kodama and N. Gokon, "Thermochemical cycles for high-temperature solar hydrogen production," *Chemical Reviews*, vol. 107, no. 10, pp. 4048–4077, 2007.

[18] M. Lundberg, "Model calculations on some feasible two-step water splitting processes," *International Journal of Hydrogen Energy*, vol. 18, no. 5, pp. 369–376, 1993.

[19] K. Ehrensberger, P. Kuhn, V. Shklover, and H. R. Oswald, "Temporary phase segregation processes during the oxidation of $(Fe_{0.7}Mn_{0.3})_{0.99}O$ in N_2-H_2O atmosphere," *Solid State Ionics*, vol. 90, no. 1–4, pp. 75–81, 1996.

[20] M. M. Bobek, R. C. Stehle, and D. W. Hahn, "Investigation of iron oxide morphology in a cyclic redox: water splitting process for hydrogen generation," *Materials*, vol. 5, no. 10, pp. 2003–2014, 2012.

[21] Y. Tamaura, A. Steinfeld, P. Kuhn, and K. Ehrensberger, "Production of solar hydrogen by a novel, 2-step, water-splitting thermochemical cycle," *Energy*, vol. 20, no. 4, pp. 325–330, 1995.

[22] N. Gokon, T. Hasegawa, S. Takahashi, and T. Kodama, "Thermochemical two-step water-splitting for hydrogen production using Fe-YSZ particles and a ceramic foam device," *Energy*, vol. 33, no. 9, pp. 1407–1416, 2008.

[23] K. S. Go, S. R. Son, and S. D. Kim, "Reaction kinetics of reduction and oxidation of metal oxides for hydrogen production," *International Journal of Hydrogen Energy*, vol. 33, no. 21, pp. 5986–5995, 2008.

[24] K. Ehrensberger, A. Frei, P. Kuhn, H. R. Oswald, and P. Hug, "Comparative experimental investigations of the water-splitting reaction with iron oxide $Fe_{1-y}O$ and iron manganese oxides $(Fe_{1-x}Mn_x)_{1-y}O$," *Solid State Ionics*, vol. 78, no. 1-2, pp. 151–160, 1995.

[25] J. R. Scheffe, A. H. McDaniel, M. D. Allendorf, and A. W. Weimer, "Kinetics and mechanism of solar-thermochemical H_2 production by oxidation of a cobalt ferrite-zirconia composite," *Energy and Environmental Science*, vol. 6, no. 3, pp. 963–973, 2013.

[26] N. Gokon, K. Kondo, T. Hatamachi, M. Sato, and T. Kodama, "Oxygen-releasing step of nickel ferrite based on Rietveld analysis for thermochemical two-step water-splitting," *International Journal of Hydrogen Energy*, vol. 38, no. 12, pp. 4935–4944, 2013.

[27] R. R. Bhosale, R. V. Shende, and J. A. Puszynski, "Thermochemical water-splitting for H_2 generation using sol-gel derived Mn-ferrite in a packed bed reactor," *International Journal of Hydrogen Energy*, vol. 37, no. 3, pp. 2924–2934, 2012.

[28] A. G. Merzhanov and A. E. Averson, "The present state of the thermal ignition theory: an invited review," *Combustion and Flame*, vol. 16, no. 1, pp. 89–124, 1971.

[29] E. N. Coker, J. A. Ohlhausen, A. Ambrosini, and J. E. Miller, "Oxygen transport and isotopic exchange in iron oxide/YSZ thermochemically-active materials via splitting of $C(^{18}O)_2$ at high temperature studied by thermogravimetric analysis and secondary ion mass spectrometry," *Journal of Materials Chemistry*, vol. 22, no. 14, pp. 6726–6732, 2012.

[30] S. Lorentzou, K. Karadimitra, C. Agrafiotis, and A. G. Konstandopoulos, "New routes for ferrite powders synthesis," in *Proceedings of the International Conference for Particle Technology (PARTEC '04)*, Nuremberg, Germany, March 2004.

[31] C. C. Agrafiotis, C. Pagkoura, A. Zygogianni, G. Karagiannakis, M. Kostoglou, and A. G. Konstandopoulos, "Hydrogen production via solar-aided water splitting thermochemical cycles: combustion synthesis and preliminary evaluation of spinel redox-pair materials," *International Journal of Hydrogen Energy*, vol. 37, no. 11, pp. 8964–8980, 2012.

[32] F. Fresno, R. Fernández-Saavedra, M. Belén Gómez-Mancebo et al., "Solar hydrogen production by two-step thermochemical cycles: evaluation of the activity of commercial ferrites," *International Journal of Hydrogen Energy*, vol. 34, no. 7, pp. 2918–2924, 2009.